Published in "Chemical Papers 71 (10): 1809–1823, 2017"
which should be cited to refer to this work.

Different molecular assemblies in two new phosphoric triamides with the same $C(O)NHP(O)(NH)_2$ skeleton: crystallographic study and Hirshfeld surface analysis

Anahid Saneei[1] · Mehrdad Pourayoubi[1] · Titus A. Jenny[2] · Aurelien Crochet[3] · Katharina M. Fromm[3] · Ekaterina S. Shchegravina[4]

Abstract Different molecular assemblies were compared in two new structures $[4\text{-}CH_3\text{-}C_6H_4C(O)NH]P(O)[NH]_2(\text{-}CH_2)_3$, **1**, and $[4\text{-}CH_3\text{-}C_6H_4C(O)NH]P(O)[NHC_6H_3(3,4\text{-}CH_3)_2]_2$, **2**, belonging to the families of "cyclic phosphoric triamide" and "phosphoric triamide", respectively. The differences in the hydrogen bond motifs were discussed (by single crystal X-ray diffraction) as a result of three factors: (1) action of two N atoms with a non-planar environment in **1** as an H-bond acceptor, (2) different orientations of three N–H bond vectors in two molecules and (3) different conformations of C=O and P=O groups. These differences lead to more complicated hydrogen bond pattern of **1,** with respect to that of **2,** as structure **1** may be considered as a model of four-acceptor–three-donor versus a two-acceptor–three-donor system in **2**. The main discrepancies of **1** and **2**, monitored by the Hirshfeld surface analysis, are related to the contribution portions of O···H/H···O contacts, in which compound **1** not only involves the greater existence of classical hydrogen bonds but also contains the further C–H···O weak interactions in its crystal packing with respect to compound **2**. Instead, in **2**, the shortage of O···H/H···O contacts has been partially compensated by the C···H/H···C interactions, due to the presence of more unsaturated carbon acceptors. The differences in assemblies are also reflected in the solid-state IR spectra, especially for the N–H vibration frequencies. The new compounds were further studied by 1D NMR experiments (^1H, ^{13}C, ^{31}P), 2D NMR techniques [HMQC and HMBC (H–C correlation), HSQC (N–H correlation)], high-resolution ESI–MS, EI–MS spectrometry and IR spectroscopy.

Keywords Phosphoric triamide · Molecular assembly · Hydrogen bonding pattern · Hirshfeld surface analysis · NMR spectroscopy

CCDC 1417623 and 1045702 contain the supplementary crystallographic data for **1** and **2**. These data can be obtained free of charge via http://www.ccdc.cam.ac.uk/conts/retrieving.html, or from the Cambridge Crystallographic Data Centre, 12 Union Road, Cambridge CB2 1EZ, UK; fax: (+44) 1223-336-033, or e-mail: deposit@ccdc.cam.ac.uk.

✉ Mehrdad Pourayoubi
pourayoubi@um.ac.ir

[1] Department of Chemistry, Faculty of Sciences, Ferdowsi University of Mashhad, P.O. Box: 9177948974, Mashhad, Iran

[2] Department of Chemistry, University of Fribourg, Rte du Musée 9, 1700 Fribourg, Switzerland

[3] Fribourg Centre for Nanomaterial's, FriMat, University of Fribourg, Chemin du Musée 3, 1700 Fribourg, Switzerland

[4] Department of Organic Chemistry, UNN Lobachevsky State University, Gagarin av., 23, Nizhny Novgorod, Russia

Introduction

Supramolecular chemistry is a highly interdisciplinary field of science that has brought together investigators from many disciplines including chemistry, physics and biology (Desiraju 2010; Resnati et al. 2015). The engineering of molecular crystals as well as the construction of supramolecular assemblies are both concerned with intermolecular interactions and hence are conceptually connected (Braga and Grepioni 1997). There is no doubt that the intermolecular contacts, especially hydrogen bonds, play a fundamental role in crystal engineering and stabilization of crystalline solids (Prins et al. 2001; Steiner 2002; Metrangolo and Resnati 2008)

and thus it is crucial to distinguish different types of interactions in any design strategy (Resnati et al. 2015).

In recent years, phosphoramides have attracted attention in the viewpoint of crystal engineering (Pourayoubi et al. 2014). The reasons for such interests are not only because they may be considered as small molecular models of some biologically active macromolecules such as phosphorus–nitrogen compounds like tetrapeptide-based phosphoramides (Wu and Hu 2016), but also because there are many examples of biologically active phosphoramide small molecules (Upadhyay, 2012). On the other hand, the basic skeleton in the phosphoramide compounds, P(=O)(N), is similar to the group occurring in peptides, (C=O)(N), and some similarity was found on the properties (Yizhak et al. 2013) with differences arising from the tetrahedral environment in phosphorus and the planar environment in carbon, and also the greater electron-donor capability of P=O with respect to C=O (Toghraee et al. 2011). Moreover, the study of intermolecular interactions received by a phosphoramide small molecule is interesting, as they are usually similar to the case where such a molecule is placed in a biological environment such as an enzyme's active site (Carletti et al. 2013).

For the study of intermolecular interactions, apart from a traditional numerical analysis based on donor–acceptor distances for the characteristic contacts, the investigation can also be done using Hirshfeld surface analysis which is a new tool for graphical studying all interactions in a crystal combined with detailed quantitative information (McKinnon et al. 2004, 2007). This method develops the study of intermolecular interactions to all of the contacts in the structure, including the weak ones (Michalik et al. 2014). Such an analysis is more precise, as the cumulative effect of weak interactions in crystal stabilization may sometimes have more important role than the classical hydrogen bonds which merely consider the interactions between the best hydrogen donor and hydrogen acceptor sites in the crystal. Additionally, this analysis is particularly useful in studying how different substituents and functionalities can affect the crystal packing and molecular assembly behaviour (Martin et al. 2015).

Herein, we give a comparative study of molecular assemblies and intermolecular arrangements in two new compounds belonging to the "cyclic phosphoric triamide" and "phosphoric triamide" families. Different hydrogen-bonded graph-set motifs and the complete superstructures of compounds are discussed, and the details of cooperation/competition of segments of molecules involved in intermolecular contacts are analysed with X-ray crystallography combined with 3D-Hirshfeld surface maps and 2D-fingerprint plots. The newly synthesized compounds are also studied by ^{1}H, ^{13}C, ^{31}P, ^{1}H–^{13}C HMQC, ^{1}H–^{13}C HMBC and ^{1}H–^{15}N HSQC NMR, ESI–MS, EI–MS spectrometry and IR spectroscopy.

Experimental

X-Ray measurements

Data collection processes were performed for the structures **1** (using Mo-Kα radiation, $\lambda = 0.71073$ Å) and **2** (using Cu-Kα radiation, $\lambda = 1.54186$ Å) with a STOE IPDS II diffractometer and a graphite monochromator. The structures were solved with SIR92 (Altomare et al. 1994) (for **1**) and SUPERFLIP (Palatinus and Chapuis 2007) (for **2**) and refined using full matrix least squares on F^2 with the SHELXL2014 (Sheldrick 2015). All hydrogen atoms were included in the refinement at geometrically fixed positions and refined with a riding model (Sheldrick 2008). The molecular graphics were generated by MERCURY (Macrae et al. 2008) and DIAMOND (Brandenburg and Putz 1999) for Windows.

Hirshfeld surface analysis

Historically, the Hirshfeld surface (HS) emerged from an effort to define the space occupied by a molecule in a crystal for the purpose of partitioning crystalline electron density into molecular fragments (Spackman and Byrom 1997). Such a surface was named in honour of F. L. Hirshfeld, who introduced the "stockholder partitioning" scheme (Hirshfeld 1977). Afterwards, it was realized that the Hirshfeld surfaces possessed a number of attributes that make them attractive for identification of intermolecular interactions in the context of crystal packing (McKinnon et al. 2004). In a Hirshfeld surface, the parameters d_e and d_i describe the distances from a point on the surface to the nearest nucleus outside and inside the surface, respectively. The d_{norm} value is the sum of the normalised quantities of d_i and d_e by considering the van der Waals radius of atoms involved. This value graphically highlights the regions of the surface involved in a specific type of intermolecular contact by a coloured scheme: red regions represent contacts shorter than the sum of van der Waals radii; white regions represent intermolecular distances close to van der Waals contacts and blue regions represent contacts longer than the sum of van der Waals radii (Spackman and Jayatilaka 2009). The fingerprint plots (FPs) are introduced as the two-dimensional representations of the information provided by the generated HSs. The FPs are plotted on an XY-grid formed by d_e, d_i pairs ($X = d_i$ and $Y = d_e$), where the frequencies of occurrence of interactions (the number of points with a given d_e, d_i pair) are represented by different colours. Moreover, the complementary regions are visible in the FPs where one molecule acts as a donor ($d_e > d_i$) and the other as an acceptor ($d_e < d_i$) (Spackman and McKinnon 2002).

Spectroscopic measurements

IR spectra of **1** and **2** were recorded using a Buck 500 scientific spectrometer as KBr pellets. ^{1}H, ^{13}C, and ^{31}P NMR spectra were recorded on a Bruker Avance 300 and a Bruker Avance III 500 spectrometer. The chemical shifts were determined relative to TMS for ^{1}H and ^{13}C, and relative to 85% H_3PO_4 for ^{31}P, as an internal or external standard, respectively. ^{1}H–^{13}C HMQC and ^{1}H–^{13}C HMBC were carried out on a Bruker Avance III 500 spectrometer, and ^{1}H–^{15}N HSQC experiments were carried out on Agilent DDR2 400 spectrometer. The mass spectra were recorded with a MS model CH7A Varian (EI, 70 eV) and a MS model 5973 Network Mass Selective Detector (EI, 20 eV). High-resolution mass spectra were recorded on a Bruker FTMS 4.7 T BioAPEX II spectrometer.

Chemicals

4-Methylbenzamide, 1,3-propanediamine, 3,4-dimethylaniline, phosphorus pentachloride, phosphorus pentoxide, acetonitrile and methanol were commercially available and chloroform was dried with P_2O_5 and distilled prior to use.

General procedure for the synthesis of compounds 1 and 2

4-CH_3-$C_6H_4C(O)NHP(O)Cl_2$ was prepared according to the method used for the analogous compound 4-NO_2-$C_6H_4C(O)NHP(O)Cl_2$ by using 4-CH_3-$C_6H_4C(O)NH_2$ instead of 4-NO_2-$C_6H_4C(O)NH_2$ (Pourayoubi and Sabbaghi 2009). To synthesize compounds **1** and **2** (the related chemical structures are shown in Table 1), a solution of

Table 1 2D ^{1}H–^{13}C HMQC and HMBC correlations for **1** and **2**

Chemical structure of compound	Atom	HMQC	HMBC	
		^{1}J	^{2}J	^{3}J
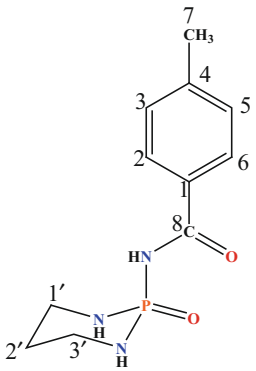 **1**	H2/H6 (δ = 7.87)	C2/C6 (δ = 127.94)	–	C4 (δ = 141.81)
			–	C8 (δ = 168.45)
	H3/H5 (δ = 7.27)	C3/C5 (δ = 128.69)	–	C1 (δ = 131.01)
			–	C7 (δ = 20.89)
	H7 (δ = 2.36)	C7 (δ = 20.89)	C4 (δ = 141.81)	C3/C5 (δ = 128.69)
	H1′/H3′ (δ = 3.05 – 3.15)	C1′/C3′ (δ = 41.76)	C2′ (δ = 26.02)	–
	H2′ (δ = 1.55 – 1.61)	C2′ (δ = 26.02)	C1′/C3′ (δ = 41.76)	–
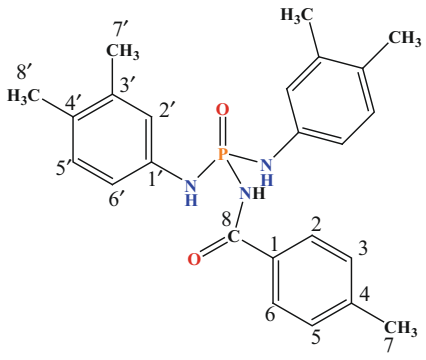 **2**	H2/H6 (δ = 7.84)	C2/C6 (δ = 128.07)	C3/C5 (δ = 128.75)	C4 (δ = 142.35)
				C8 (δ = 167.53)
	H3/H5 (δ = 7.26)	C3/C5 (δ = 128.75)	C4 (δ = 142.35)	C1 (δ = 130.41)
			C2/C6 (δ = 128.07)	C7 (δ = 20.89)
	H7 (δ = 2.34)	C7 (δ = 20.89)	C4 (δ = 142.35)	C3/C5 (δ = 128.75)
	H2′ (δ = 6.96)	C2′ (δ = 119.02)	C1′ (δ = 138.74)	C4′ (δ = 127.85)
	H5′ (δ = 6.91)	C5′ (δ = 129.54)	C6′ (δ = 115.14)	C1′ (δ = 138.74)
				C3′ (δ = 136.10)
	H6′ (δ = 6.87)	C6′ (δ = 115.14)	C1′ (δ = 138.74)	C4′ (δ = 127.85)
	H7′ (δ = 2.11)	C7′ (δ = 19.50)	C3′ (δ = 136.10)	C2′ (δ = 119.02)
				C4′ (δ = 127.85)
	H8′ (δ = 2.08)	C8′ (δ = 18.37)	C4′ (δ = 127.85)	C3′ (δ = 136.10)

2 mmol diamine (1,3-propanediamine) for **1** and 4 mmol amine (3,4-dimethylaniline) for **2** in dry $CHCl_3$ (5 mL) was added dropwise to a stirred solution of 1 mmol 4-CH_3-$C_6H_4C(O)NHP(O)Cl_2$ in dry $CHCl_3$ (20 mL) at 0 °C. After 4 h, the solvent was removed in vacuum and the solid was washed with H_2O. Suitable single crystals for X-ray crystallography were obtained at room temperature from a mixture of $CH_3OH/CHCl_3$ (1:1) for **1** and CH_3OH/CH_3CN (3:1) for **2** (after a few days).

Spectroscopic data

4-Methyl-N-(2-oxido-1,3,2-diazaphosphinan-2-yl) benzamide, 1

M.p. 218 °C. ESI–MS = 254.10508. (calcd. for $C_{11}H_{17}N_3O_2P^+$ 254.10529). $^{31}P\{^1H\}$ NMR (121.49 MHz, DMSO-d_6, 85% H_3PO_4): δ = 3.52 (*s*). ^1H NMR (500.13 MHz, DMSO-d_6, TMS): δ = 9.10 (very br. *s*, 1H, CONH), 7.87 (apparent *d*, *J* = 8.2 Hz, 2H, H2/H6), 7.27 (apparent *d*, *J* = 7.9 Hz, 2H, H3/H5), 4.49 (*m*, 2H, NH), 3.15–3.05 (*m*, 4H, H1′/H3′), 2.36 (*s*, 3H, H7), 1.61–1.55 (*m*, 2H, H2′). ^{13}C NMR (125.76 MHz, DMSO-d_6, TMS): δ = 168.45 (*s*, C8), 141.81 (*s*, C4), 131.01 (*d*, $^3J_{PC}$ = 7.4 Hz, C1), 128.69 (*s*, C3/C5), 127.94 (*s*, C2/C6), 41.76 (*d*, $^2J_{PC}$ = 3.5 Hz, C1′/C3′), 26.02 (*d*, $^3J_{PC}$ = 6.2 Hz, C2′), 20.89 (*s*, C7). $^{15}N–^1H$ corr. (DMSO-d_6) {–283.16, 4.52} (CH_2NHPO) (CONHPO correlation peak was not detected). IR (KBr, cm^{-1}): 3318, 3156, 2930, 2874, 1660 (C=O), 1460, 1271, 1219, 1194, 1095, 998, 822, 742. MS (70 eV, EI): *m/z* (%) = 30 (84), 43 (73), 56 (87), 72 (88), 91 (90), 117 (87), 119 (95), 135 (100), 136 (88), 155 (22), 181 (23), 251 (88), 252 (84), 253 (13).

N-(Bis((3,4-dimethylphenyl)amino)phosphoryl)-4-methylbenzamide, 2

M.p. 248 °C. ESI–MS: 422.19962 (calcd. for $C_{24}H_{29}N_3O_2P^+$ 422.19919). $^{31}P\{^1H\}$ NMR (121.49 MHz, DMSO-d_6, 85% H_3PO_4): δ = −4.48 (*s*). Mixture of rotamers (Major rotamer): ^1H NMR (500.13 MHz, DMSO-d_6, TMS): δ = 9.73 (*d*, $^2J_{PH}$ = 8.3 Hz, 1H, CONH), 7.84 (apparent *d*, *J* = 8.3 Hz, 2H, H2/H6), 7.55 (*d*, $^2J_{PH}$ = 9.5 Hz, 2H, NH), 7.26 (apparent *d*, *J* = 7.9 Hz, 2H, H3/H5), 6.96 (*d*, *J* = 1.9 Hz, 2H, H2′), 6.91 (*d*, *J* = 8.2 Hz, 2H, H5′), 6.87 (*dd*, *J* = 8.1, 2.1 Hz, 2H, H6′), 2.34 (*s*, 3H, H7), 2.11 (*s*, 6H, H7′), 2.08 (*s*, 6H, H8′). ^{13}C NMR (125.76 MHz, DMSO-d_6, TMS): δ = 167.53 (*s*, C8), 142.35 (*s*, C4), 138.74 (*s*, C1′), 136.10 (*s*, C3′), 130.41 (*d*, $^3J_{PC}$ = 8.8 Hz, C1), 129.54 (*s*, C5′), 128.75 (*s*, C3/C5), 128.07 (*s*, C2/C6), 127.85 (*s*, C4′), 119.02 (*d*, $^3J_{PC}$ = 7.4 Hz, C2′), 115.14 (*d*, $^3J_{PC}$ = 7.4 Hz, C6′), 20.89 (*s*, C7), 19.50 (*s*, C7′), 18.37 (*s*, C8′). $^{15}N–^1H$ corr. (DMSO-d_6) {–258.09, 9.78} (CONHPO), {−248.80, 7.64} ($C_{Ar}NHPO$) (Minor rotamer): ^1H NMR (500.13 MHz, DMSO-d_6, TMS): δ = 9.54 (*d*, $^2J_{PH}$ = 8.7 Hz, CONH), 7.81 (apparent *d*, *J* = 8.3 Hz, H2/H6), 7.41 (broad, NH), 7.23 (apparent *d*, *J* = 8.0 Hz, H3/H5), 6.96 (*d*, H2′), 6.91 (*d*, *J* = 7.4 Hz, H5′), 6.84 (*dd*, H6′), 2.33 (*s*, 3H, H7), 2.13 (*s*, 6H, H7′), 2.09 (*s*, 6H, H8′). ^{13}C NMR (125.76 MHz, DMSO-d_6, TMS): δ = 167.33 (*s*, C8), 142.00 (*s*, C4), 139.28 (*s*, C1′), 135.84 (*s*, C3′), 130.68 (*d*, $^3J_{PC}$ = 8.6 Hz, C1), 129.95 (*s*, C5′), 128.67 (*s*, C3/C5), 128.01 (*s*, C2/C6), 127.13 (*s*, C4′), 118.61 (*d*, $^3J_{PC}$ = 7.6 Hz, C2′), 114.75 (*d*, $^3J_{PC}$ = 7.4 Hz, C6′), 20.86 (*s*, C7), 19.39 (*s*, C7′), 18.44 (*s*, C8′). $^{15}N–^1H$ corr. (DMSO-d_6) {–258.60, 9.77} (CONHPO), {−249.55, 7.61} ($C_{Ar}NHPO$). IR (KBr, cm^{-1}): 3280, 3097, 2919, 1646 (C=O), 1615, 1511, 1442, 1393, 1359, 1279, 1225, 1165, 1116, 1016, 969, 923, 863, 817, 748, 685. MS (20 eV, EI): *m/z* (%) = 41 (47), 51 (40), 63 (34), 77 (43), 91 (63), 106 (89), 117 (64), 119 (32), 121 (100), 129 (3), 139 (6), 152 (10), 167 (5), 181 (9), 196 (3), 211 (9), 223 (3), 231 (3), 243 (13), 257 (1), 271 (3), 286 (3), 301 (12), 303 (3), 304 (9), 421 (8). Experimental NMR, IR and Mass spectra of compounds **1** and **2** are given in the Electronic Supplementary Information (ESI).

Results and discussion

Mass spectrometric analysis

The high-resolution ESI–MS characterization was carried out for two compounds, which very much supported the presented structures.

The EI mass spectra of compounds **1** and **2** were also recorded, which show the molecular ion peaks $[M]^+$ at *m/z* 253 and 421, respectively. Compound **1** presents the $[M-1]^+$ fragment peak which can be attributed to loss of an H atom. The peak at *m/z* 117 in the mass spectra of two compounds is assigned to the 4-CH_3-$C_6H_4CN^+$ radical-cation which was formed by the removing of amidophosphoric acid from the parent ion, as was reported for analogous $[C_6H_5C(O)NH]P(O)[OR]_2$ phosphoramides by the removing of the esters of phosphoric acid (Mizrahi and Modro 1982). The observation of this fragment indicates that the parent radical-cation rapidly undergoes a migration of phosphorous from nitrogen to oxygen. From this resulting isomer a McLafferty fragmentation would produce the $C_8H_7N^+$ radical cation and neutral amidophosphoric acid. Typical for the McLafferty fragmentation is the fact that the charge could appear alternatively on either fragment, i.e. the amidophosphoric acid part could also be charged and hence observed. Typically, the signal related to amidophosphoric acid radical-cation was detected in the mass spectrum of **2** (m/z 304,

(HO)P(O)[NHC_6H_3-3,4-$(CH_3)_2]_2^+$) after loss of 4-CH_3-C_6H_4CN. It is concluded that the pathway involving elimination of amidophosphoric acid molecule is preferred in **2**, due to a considerable lower intensity of the amidophosphoric acid radical-cation compared to the 4-methyl-phenyl cyanide radical-cation in compound **2**.

For compound **2**, the peaks at *m/z* of 303 (assigned to the ion (O)P(O)[NHC_6H_3-3,4-$(CH_3)_2]_2^+$) and at 286 ([M $-C_8H_9NO]^+$) are also revealed. The base peaks for compounds **1** and **2** are observed, respectively, at *m/z* of 135 (related to the 4-CH_3-$C_6H_4C(O)NH_2^+$ ion) which results through a classical onium reaction (Bauerschmidt et al. 1992) and 121 (attributed to the 3,4-$(CH_3)_2$-$C_6H_3NH_2^+$ fragment ion).

The other important peak in these compounds appears at *m/z* 119, which is evidence for a bond scission of the amide bond in the NH–C(O) section generating the CH_3-$C_6H_4C(O)^+$ fragment, as reported for analogous compounds (Gholivand et al. 2008).

IR and NMR study

Stretching frequencies of the N–H units occur at 3156 and 3318 cm^{-1} for **1** and 3097 and 3280 cm^{-1} for **2**. In both compounds, the lower stretching frequencies are related to N_{CP}–H, engaged in hydrogen bonding interactions with the P=O group (with greater hydrogen bond strengths with respect to the N_P–H···O=C hydrogen bond), as demonstrated by a comparison of IR spectra in various compounds and supported by quantum chemical calculations (Pourayoubi et al. 2013). The reason for the higher N_P–H stretching frequency of **1** with respect to that of **2** is related to the involvement of N_P–H units in weaker hydrogen bonds as will be discussed in the X-ray crystallography section.

The phosphorus chemical shifts for **1** and **2** are observed at 3.52 and −4.48 ppm, respectively. The negative value for **2** may be attributed to the magnetic anisotropy of aromatic rings (of two NHC_6H_3-3,4-$(CH_3)_2$ groups) on the phosphorus atom existing in the cone-shaped shielding zone. Such negative values of phosphorus chemical shifts were also found in the ^{31}P NMR of analogous compounds, which typically include NHC_6H_4-4-CH_3 group bonded to P atom, for example: [4-F-$C_6H_4C(O)NH]P(O)[NHC_6H_4$-4-$CH_3]_2$ (−4.61 ppm) (Tarahhomi et al. 2011) and [$CF_3C(O)NH]P(O)[NHC_6H_4$-4-$CH_3]_2$ (−5.38 ppm) (Gholivand et al. 2009).

Table 1 lists the ^{1}H and ^{13}C NMR assignments of both compounds, with the assignments achieved by 2D experiments. In the ^{1}HNMR spectrum of **1** the broad signal at 9.10 ppm is related to the corresponding C(O)NHP(O) proton. For **2**, a similar proton is revealed as a doublet signal at 9.73 ppm with $^2J_{PNH} = 8.3$ Hz. Compound **2** also shows a set of minor signals attributed to the other rotamer in solution, whereby we bring here the minor signal for NH at 9.54 ppm with $^2J_{PNH} = 8.7$ Hz. The two rotameric forms interconvert slowly on the NMR time scale.

The multiplet signal at 4.49 ppm for **1** corresponds to two chemically equivalent N_P–H protons in the P(O)$[NH]_2(CH_2)_3$ segment. For **2**, the fluxionality would explain why not only two signals at 7.41 ppm and 7.55 ppm are observed for the N_P–H protons of the P(O)[NHC_6H_3-3,4-$(CH_3)_2]_2$ segment, but also why the first signal is so broad. The full assignments of major rotamer are also represented in Table 1.

The aromatic protons of the 4-CH_3-$C_6H_4C(O)$ segment are revealed as two doublet signals in **1** and as two sets of two doublets in **2**, in the range of 7.23–7.87 ppm.

In the ^{13}C NMR spectrum of **1**, the doublet signal at 131.01 ppm ($^3J_{PC} = 7.4$ Hz) is related to the C1 atom of 4-CH_3-C_6H_4 segment. For the major and minor rotameric forms of **2**, the signal of similar C atom is also split as doublets at 130.41 ($^3J_{PC} = 8.8$ Hz) and 130.68 ppm ($^3J_{PC} = 8.6$ Hz), respectively.

Furthermore, the carbon atoms of $[NH]_2(CH_2)_3$ part in **1** show both $^2J_{PC}$ (at 41.76 ppm) and $^3J_{PC}$ (at 26.02 ppm) in the observed doublet signals. For **2**, the signals of NHC_6H_3(3,4-$CH_3)_2$ part include only doublets at 119.02 and 115.14 ppm for major rotamer and at 118.61 and 114.75 ppm for minor rotamer related to three-bond separation phosphorus-carbon coupling ($^3J_{PC}$), besides the singlets for the other carbon atoms.

Moreover, the data of 2D ^{1}H–^{13}C HMQC and ^{1}H–^{13}C HMBC techniques were gathered in Table 1 in order to provide information about the interaction between the protons and the carbon atoms, which are directly attached to each other (via HMQC) and also for assignment of the carbon atoms not-bonded to the hydrogen atom (via HMBC) in compounds **1** and **2**. The latter spectrum shows the connectivities between proton and carbon atoms with ^2J and ^3J relations.

Additionally, in the ^{1}H–^{15}N HSQC NMR spectra of **1** and **2** the following cross-peaks could be found: 4.52/–283.16 ppm for N_P–H of **1** and 7.64/−248.80 ppm and 7.61/−249.55 ppm for N_P–H in two rotameric forms of **2**. The cross-peak of N_{CP}–H in is absent **1**, while two rotameric forms of **2** manifest the peaks at 9.78/−258.09 ppm and 9.77/−258.60 ppm. The disappearance of cross-peak noted for **1** may be due to the hydrogen bond formation in solution.

X-ray crystallography investigation

General structural features

Both compounds **1** and **2** crystallize in the monoclinic crystal system, within the $P2_1/c$ space group. The

Table 2 Crystal data and structure refinement for **1** and **2**

	1	**2**
Empirical formula	$C_{11}H_{16}N_3O_2P$	$C_{24}H_{28}N_3O_2P$
Formula weight	253.24	421.46
Temperature (K)	200(2)	200(2)
Wavelength (Å)	0.71073	1.54186
Crystal system	Monoclinic	Monoclinic
Space group	$P2_1/c$	$P2_1/c$
Unit cell dimensions	$a = 13.5749(5)$ Å	$a = 9.9002(6)$ Å
	$b = 10.2937(4)$ Å	$b = 19.0319(11)$ Å
	$c = 9.3410(8)$ Å	$c = 12.1900(8)$ Å
β (°)	107.846(5)	95.531(5)
Volume (Å^3)	1242.47(13)	2286.1(2)
Z	4	4
Density (calculated) (g/cm^3)	1.354	1.225
Absorption coefficient (mm^{-1})	0.216	1.257
F(000)	536	896
Index ranges	$-16 \le h \le 15$, $-12 \le k \le 12$, $-10 \le l \le 11$	$-11 \le h \le 11$, $-20 \le k \le 22$, $-14 \le l \le 14$
Reflections collected	15,290	16,550
Independent reflections	2161 [$R_{(int)} = 0.0875$]	3780 [$R_{(int)} = 0.0844$]
Refinement method	Full-matrix least-squares on F^2	Full-matrix least-squares on F^2
Data/restraints/parameters	2161/0/165	3780/0/285
Goodness-of-fit on F^2	1.062	1.018
Final R indices [$I > 2\sigma(I)$]	$R_1 = 0.0796$, $wR_2 = 0.2100$	$R_1 = 0.0450$, $wR_2 = 0.1232$
R indices (all data)	$R_1 = 0.0947$, $wR_2 = 0.2211$	$R_1 = 0.0479$, $wR_2 = 0.1250$
Largest diff. peak and hole (e Å^{-3})	0.681 and −0.984	0.333 and −0.346

crystallographic data and refinement parameters are presented in Table 2. The asymmetric units of the two compounds contain one molecule each (Figs. 1, 2). The bond angles at the P atoms are in agreement with a distorted tetrahedral configuration with calculated τ4 geometry index values (Yang et al. 2007) of 0.94 (for **1**) and 0.92 (for **2**). In both structures, the O=P–N_{CP} angles are smaller than the two O=P–N_P angles, Table 3 (in our discussion, the N_{CP} is used for the nitrogen atom within the C(O)NHP(O) segment and the N_P is representation of two other nitrogen atoms attached to the phosphorous atom). The P=O and C=O bond lengths [respectively, 1.464(3) Å and 1.235(6) Å for **1** and 1.4734(11) Å and 1.228(2) Å for **2**] are in the standard range for phosphoric triamides (Toghraee et al. 2011). The six-membered P1/N1/C3/C2/C1/N2 ring of **1** adopts a nearly half-boat conformation on the basis of puckering parameters calculated according to Cremer and Pople (1975) [$Q = 0.500(6)$, $\theta = 155.1(6)°$, $\Phi = 13.9(14)°$]. The out of plane displacements calculated for the atoms of the ring are as follows: P1, −0.066(2); N1, 0.100(5); C3, −0.219(6); C2, 0.304(6); C1, −0.270(6) and N2, 0.151(5).

With respect to the nitrogen atoms, the main differences in **1** and **2** are related to the geometries at the N atoms bound to P,

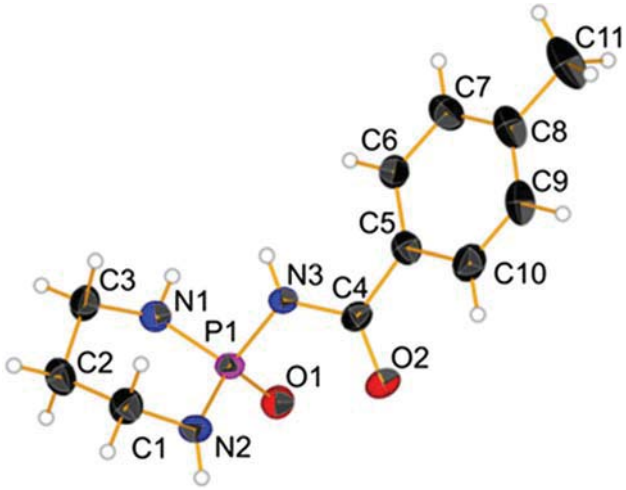

Fig. 1 Displacement ellipsoid plot (50% probability) is shown for **1** with atom numbering scheme. H atoms are drawn as spheres of arbitrary radii

calculated by the bond-angle sums at the N atoms (Σ). Structure **1** includes two N_P atoms which are located in the non-planar environment [$\Sigma = 343(3)°$ and $350(3)°$]. The criteria for distinguishing between planar and non-planar geometries are the

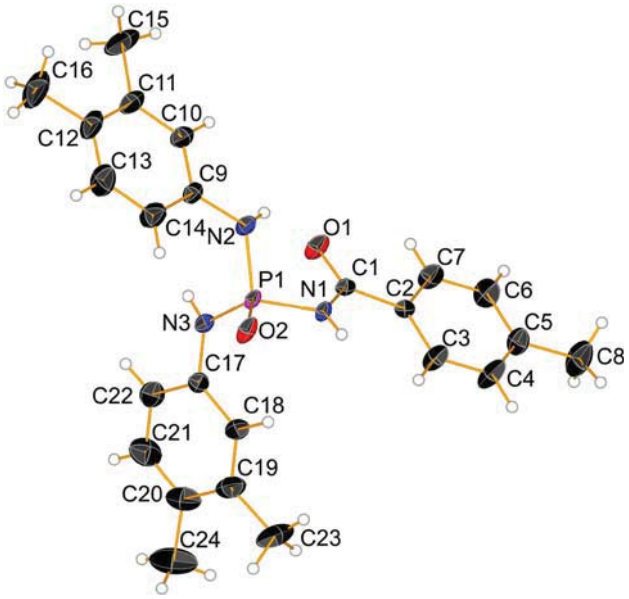

Fig. 2 Displacement ellipsoid plot (50% probability) is shown for **2** with atom numbering scheme. H atoms are drawn as spheres of arbitrary radii

Table 3 Selected bond distances (Å) and angles (°) for **1** and **2**

1			
P1=O1	1.464 (3)	P1–N1	1.627 (4)
C4=O2	1.235 (6)	P1–N2	1.632 (4)
C4–N3	1.360 (6)	P1–N3	1.685 (4)
O1=P1–N1	114.9 (2)	N1–P1–N2	106.6 (2)
O1=P1–N2	113.2 (2)	N1–P1–N3	104.8 (2)
O1=P1–N3	109.89 (19)	N2–P1–N3	106.7 (2)
O1=P1–N3–C4	−45.8 (4)	C4–N3–P1–N1	−169.9 (4)
P1–N3–C4=O2	−13.9 (6)	C4–N3–P1–N2	77.2 (4)
2			
P1=O2	1.4734 (11)	P1–N1	1.6824 (12)
C1=O1	1.228 (2)	P1–N2	1.6392 (14)
C1–N1	1.3659 (18)	P1–N3	1.6410 (13)
O2=P1–N1	108.08 (6)	N1–P1–N2	104.29 (7)
O2=P1–N2	116.11 (7)	N1–P1–N3	108.66 (7)
O2=P1–N3	113.90 (7)	N2–P1–N3	105.21 (7)
O2=P1–N1–C1	−177.11 (12)	C1–N1–P1–N2	−52.99 (13)
P1–N1–C1=O1	11.7 (2)	C1–N1–P1–N3	58.83 (14)

same as previously proposed: N(planar) and N(pyramidal) refer to the cases with $\Sigma \geq 352.5°$ and $\Sigma \leq 339.0°$, respectively, and the intermediate entries are the cases with Σ in the range 339.0°–352.5° (Allen and Bruno, 2010). In **2**, one N_P atom is in a non-planar environment [$\Sigma = 350(2)°$] and the other N_P atom indicates the planar environment [$\Sigma = 360(2)°$]. In both structures, the N_{CP} atom is practically planar.

The nitrogen atom in a planar environment shows low Lewis base characteristic and does not take part in hydrogen bonding as an acceptor, while there is a possibility (however small) that a nitrogen atom with a tendency to pyramidality acts in hydrogen bonding pattern as an acceptor. This knowledge is based on a survey on the Cambridge Structural Database (CSD, Groom et al. 2016) for the structures with a P(O)NXY segment. There is no structure with an N atom as an acceptor in the C(O)NHP(O)-based phosphoric triamides in the CSD, and a few examples are related to the other families of phosphorus–nitrogen compounds (Pourayoubi et al. 2014).

As will be discussed in the section of hydrogen bonding patterns, the number of H-acceptor sites in **1** develops to four and the structure of **2** only includes two acceptors in its hydrogen bonding pattern (Fig. 3). On the other hand, in **1** the number of H-acceptor sites is higher than the number of H-donor sites, leading to a bifurcated hydrogen bond (N–H)(···O)(···N). In **2**, with a larger number of H-donor sites than H-acceptor sites, a double-acceptor site in the (N–H···)(N–H···)O=C entity is found.

Other differences between the two structures are related to the directions of N–H bond vectors which are illustrated in Fig. 4. With respect to the plane crossing the three N atoms in **1** and **2**, two N_P–H units in the cyclic compound **1** are located nearly in the same side of the P=O group (one N_P–H units has the *syn*-orientation and the other unit has a *gauche*-orientation) and in the acyclic compound **2**, two N_P–H units adopt an *anti*-orientation relative to the P=O group. The direction of N_{CP}–H bond vector versus P=O is different from what was noted for N_P–H bond vector with respect to the P=O (i.e. *anti* in **1** and *syn* in **2**). The results of such different conformations are reflected in the various H-bonding patterns and diversity of graph-sets created which will be explained in more detail in the next section.

Hydrogen bonding pattern

In the crystal structure of **1**, the N3–H3*C* unit takes part in a normal two-centred hydrogen bond, while surprisingly both N1–H1*C* and N2–H2*C* units are involved in the bifurcated intermolecular N–H(···O)(···N) entities. This is a novel feature of this structure and there are no C(O)NHP(O)$(NH)_2$-based phosphoric triamides in the CSD including such three-centred hydrogen bonds. The reasons for the existence of such interactions are due to the presence of nitrogen atoms in a non-planar environment and also their role as an H-acceptor. Within these two N–H units noted, N2–H2*C* is near to three acceptors, but as will be discussed in the section of Hirshfeld analysis the third neighbour separation (H2*C*···O1) is a week intermolecular contact.

The sites involving in the hydrogen bonds of **1** are three N–H units as donors (N1–H1*C*, N2–H2*C* and N3–H3*C*)

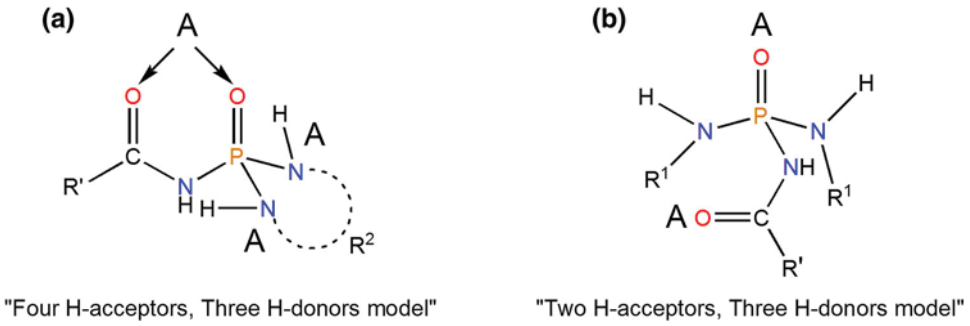

Fig. 3 A general representation for cyclic phosphoric triamide **1** (**a**) and phosphoric triamide **2** (**b**) showing the acceptor sites as specified with "A". The hydrocarbon segments attached to the carbonyl group and secondary N atoms are shown with R', R^1 and R^2. The $CH_2CH_2CH_2$ linker (R^2) is given as curved dashed line

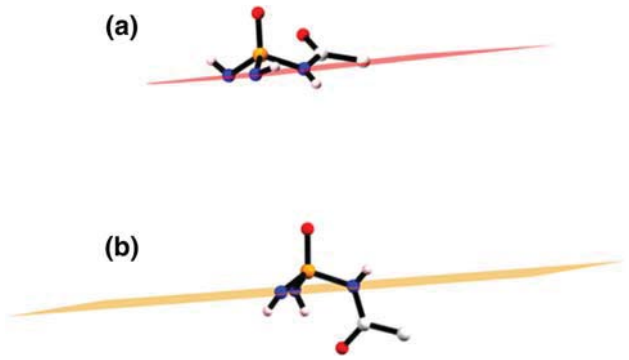

Fig. 4 The directionality of the N_P–H and N_{CP}–H bond vectors versus P=O group relative to the plane involving three N atoms (**a**) for structure **1** and (**b**) for structure **2**. Only the C–C(O)NHP(O)$(NH)_2$ segment in both structures are shown for clarity. The mean planes are shown as *red* and *orange colours*

and four sites as acceptors including two O atoms (P1=O1 and C4=O2) as well as two N atoms with relatively high deviation from planarity (N1 and N2). Considering the contacts involving these sites, a 2D grid network is built parallel to the *bc* plane (Fig. 5). The basic framework of two-dimensional arrangement is a result of cooperation between three types of hydrogen bonds (N1–H1*C*···N2^{i}, N2–H2*C*···O2^{ii} and N3–H3*C*···O1^{iii}; symmetry codes: (i) $-x+1, y+1/2, -z+3/2$, (ii) $-x+1, -y, -z+2$ and (iii) $x, -y+1/2, z-1/2$, Table 4). The other N1–H1*C*···O2^{i}, N2–H2*C*···O1^{ii} and N2–H2*C*···N2^{ii} hydrogen bonds do not extend the dimensionality of the hydrogen bond pattern; however, the 3D superstructure is a result of some weak interactions which will be discussed in the section of Hirshfeld surface analysis.

The important ring motifs, based on the hydrogen bonds noted, are shown in Fig. 6 which include $R_1^2(6)$, $R_2^2(8)$, $R_2^2(10)$ and $R_2^2(12)$. Moreover, some high-order cyclic motifs can be distinguished in the structure as well as different linear hydrogen-bonded paths.

For an example of a bigger ring motif, we bring here the $R_4^4(16)$ graph-set which is the basic building unit of the 2D arrangement. This motif is built from hydrogen bonding interactions between four adjacent molecules via N1–H1*C*···N2^{i} and N3–H3*C*···O1^{iii} hydrogen bonds (Fig. 7).

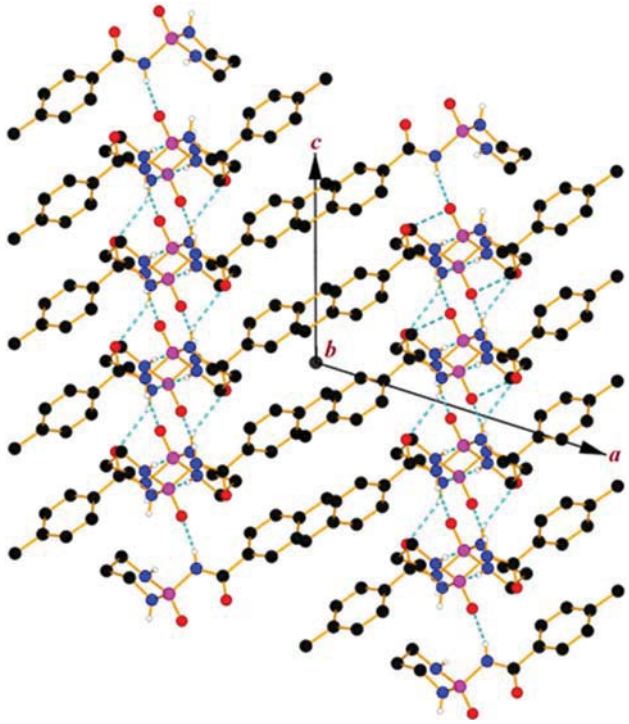

Fig. 5 A view of the two-dimensional array of **1** built from N_{CP}–H···O=P, N_P–H···O=C and N_P–H···N_P hydrogen bonds. The hydrogen bonds are shown as *dotted lines* and H atoms not involved in hydrogen bonds have been omitted for clarity

The N2–H2*C*···O2^{ii} hydrogen bond then connects the adjacent tetramers to each other.

An example of a hydrogen-bond chain graph-set in the structure **1** is shown in Fig. 8, which includes an assembly of five molecules through the N2–H2*C*···O1 and N3–H3*C*···O1 hydrogen bonds forming a zigzag $C_4^3(14)$ chain.

In addition to the hydrogen bonds discussed, the structure of **1** may be rationalized by the weak cohesion from the C–H···O (C3–H3A···O2, C···O = 3.265 Å) and C–H···π-electron ring (C2–H2A···π, H···Cg1 = 2.651 Å, Cg1 = centroid of C5/C6/C7/C8/C9/C10 ring) interactions.

The hydrogen bond pattern of **2** is relatively simple, as the nitrogen atoms do not participate as acceptors. So, the

Table 4 Hydrogen bond geometries for **1** and **2**

D–H···A	d(D–H)	d(H···A)	d(D···A)	∠(DHA)	Symmetry code
1					
N1–H1*C*···N2^{i}	0.90(5)	2.67(5)	3.531(6)	159(4)	(i) $-x + 1, y + 1/2, -z + 3/2$
N1–H1*C*···O2^{i}	0.90(5)	2.56(5)	3.114(5)	120(4)	(i) $-x + 1, y + 1/2, -z + 3/2$
N2–H2*C*···O2^{ii}	0.77(6)	2.47(6)	3.223(6)	165(5)	(ii) $-x + 1, -y, -z + 2$
N2–H2*C*···N2^{ii}	0.77(6)	2.93(5)	3.333(9)	116(5)	(ii) $-x + 1, -y, -z + 2$
N3–H3*C*···O1^{iii}	0.79(6)	2.02(6)	2.791(5)	163(5)	(iii) $x, -y + 1/2, z - 1/2$
2					
N1–H1···O2^{i}	0.79(3)	2.00(3)	2.7803(17)	171(3)	(i) $-x + 1, -y + 1, -z + 1$
N2–H2···O1	0.82(3)	2.17(3)	2.8468(17)	139(3)	
N3–H3*B*···O1^{ii}	0.84(4)	2.01(4)	2.8359(17)	170(3)	(ii) $-x, -y + 1, -z + 1$

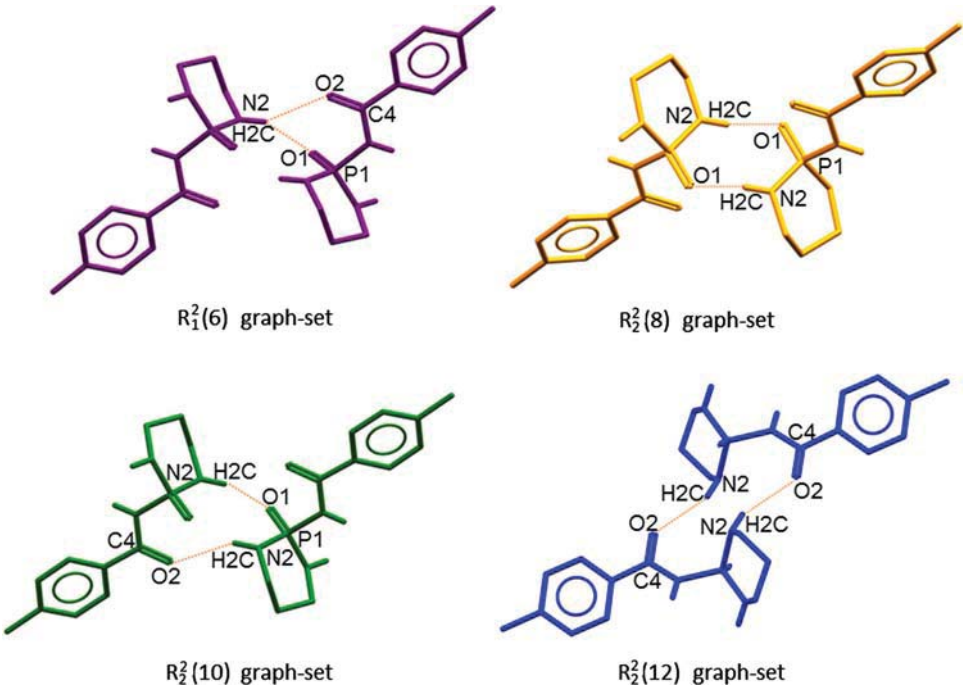

Fig. 6 Different graph-set motifs in structure **1**; H atoms bonded to the C atoms have been omitted for the sake of clarity

structure of **2** is a model of "two-acceptor–three-donor" systems. In the solid state, the molecules of **2** are hydrogen-bonded to each other making a 1D arrangement along the *a* axis, through the N_{CP}–H···O=P and N_P–H···O=C hydrogen bonds, Fig. 9, forming alternative $R_2^2(8)$ and $R_2^2(12)$ graph-sets arranged through a chain path. This arrangement also includes $S_1^1(6)$ graph-set motif made by N_P–H···O=C intramolecular hydrogen bond.

By considering intermolecular C–H···π-electron ring interactions (C8–H8B···π, H···Cg1 = 3.421 Å, Cg1 = centroid of C17/C18/C19/C20/C21/C22 ring and C23–H23C···π, H···Cg2 = 3.412 Å, Cg2 = centroid of C2/C3/C4/C5/C6/C7 ring), a 2D network parallel to (011) plane is formed by the connection of 1D hydrogen-bonded chains.

Study of intermolecular interactions by Hirshfeld surface analysis

For a better understanding of the packing maps and variety of interactions, it was decided to use a graphical tool for identification and understanding of intermolecular interactions. For this purpose, we used Hirshfeld surface (HS) analysis which is a useful method for discerning the close contacts around a component (molecule/ion).

Molecular Hirshfeld surfaces (d_{norm} and shape index) and 2D fingerprint plots of structures **1** and **2** were generated by the *CrystalExplorer* 3.1 computer program (Wolff et al. 2012). The HSs of **1** and **2** with the numerical labels for different contacts are given in Fig. 10a, b. Table 5 lists all of the contacts including the classical

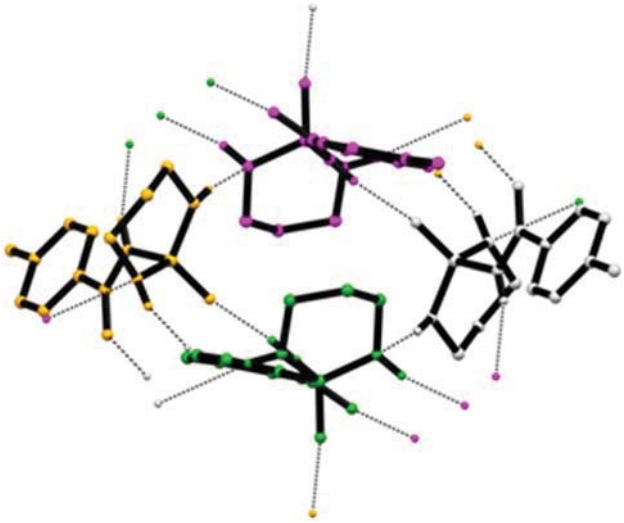

Fig. 7 Cyclic $R_4^4(16)$ tetramer motif in the crystal structure of **1**, formed via N1–H1*C*···N2^{i} and N3–H3*C*···O1^{iii} hydrogen bonds. H atoms not involved in hydrogen bonding have been omitted for clarity. The symmetry-related molecules are shown with *different colours* [symmetry codes: (i) $-x + 1, y + 1/2, -z + 3/2$, (iii) $x, -y + 1/2, z - 1/2$]

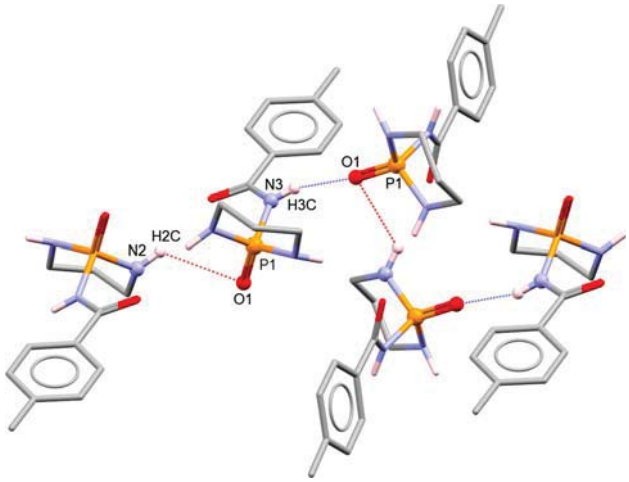

Fig. 8 The $C_4^3(14)$ chain graph-set in the crystal structure of **1**, formed via N2–H2*C*···O1^{ii} (*red dashed line*) and N3–H3*C*···O1^{iii} (*blue dashed line*) hydrogen bonds. H atoms bonded to the C atoms have been omitted for the sake of clarity [symmetry codes: (ii) $-x + 1, -y, -z + 2$, (iii) $x, -y + 1/2, z - 1/2$]

hydrogen bonds and the weak interactions, with the bold text used for the classical hydrogen bond.

The label 1 is devoted to the most important interaction in both structures (Fig. 10a, b), namely between N_{CP}–H unit and the oxygen atom of P=O group, appearing as the large red spots. The N_{CP}–H···O=P interactions have the shortest N···O distances in two structures, as was noted earlier (Table 4). In the crystal structures of **1** and **2**, there are two other N_P–H units which take part in some

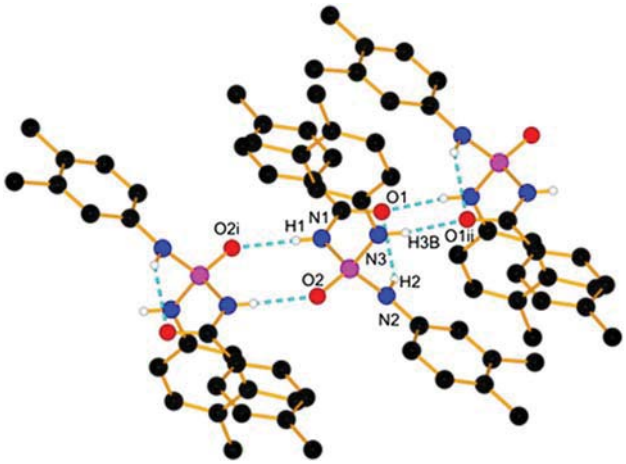

Fig. 9 A crystal packing diagram for structure **2**, formed via N1–H1···O2^{i} and N3–H3*B*···O1^{ii} hydrogen bonds (*dashed lines*). The H atoms bonded to the C atoms have been omitted for clarity [symmetry codes: (i) $-x + 1, -y + 1, -z + 1$, (ii) $-x, -y + 1, -z + 1$]

additional weak intermolecular interactions, especially N_P–H···O=C in both structures and N_P–H···N_P in **1**.

As mentioned in the section of X-ray crystallography, the N2–H2*C* unit of the $NH(CH_2)_3NH$ segment in **1** is near to three H-acceptor atoms proposing the existence of N2–H2*C*···O2=C4, N2–H2*C*···N2 and N2–H2*C*···O1=P1 contacts. The two former interactions are seen as relatively large and small red spots, respectively (labels 2 and 7 in Fig. 10a). The possible N2–H2*C*···O1=P1 interaction has the H···O distance near the corresponding sum of the van der Waals radii and thus appears as white area. The N1–H1*C* unit of the $NH(CH_2)_3NH$ segment also behaves as a double H-atom donor and takes part in N1–H1*C*···N2 (label 5, Fig. 10a) and N1–H1*C*···O2=C4 (label 6, Fig. 10a) weak intermolecular interactions. In contrast to **1**, only one of the N_P–H units in **2** participates in intermolecular hydrogen bonding (with C=O group) and revealed as a large red area in Fig. 10b (labelled 2).

There are also two kinds of weak C–H···O intermolecular interactions in compound **1**: C_{Ar}–H···O=P (label 3 in Fig. 10a), and C_{Aliph}–H···O=C (label 4 in Fig. 10a). The C_{Ar}–H···O=P contact also exists in structure **2** (label 3 in Fig. 10b). All discussed C–H···O close contacts are viewed as small red areas in the related Hirshfeld surface maps.

Figure 11a, b displays the Hirshfeld surfaces mapped with shape index functions for **1** and **2**. Shape index is a feature of Hirshfeld surface analysis that allows for identification of complementarity between molecules in the crystal packing so that features on the shape index surface that have an identical pattern but opposite colours indicate areas of intermolecular complementarity such as aromatic stacking interactions, e.g. C–H···π and π···π interactions. The red π-hole in Fig. 11a is related to the electron-rich aromatic system and indicates the presence of C–H···π

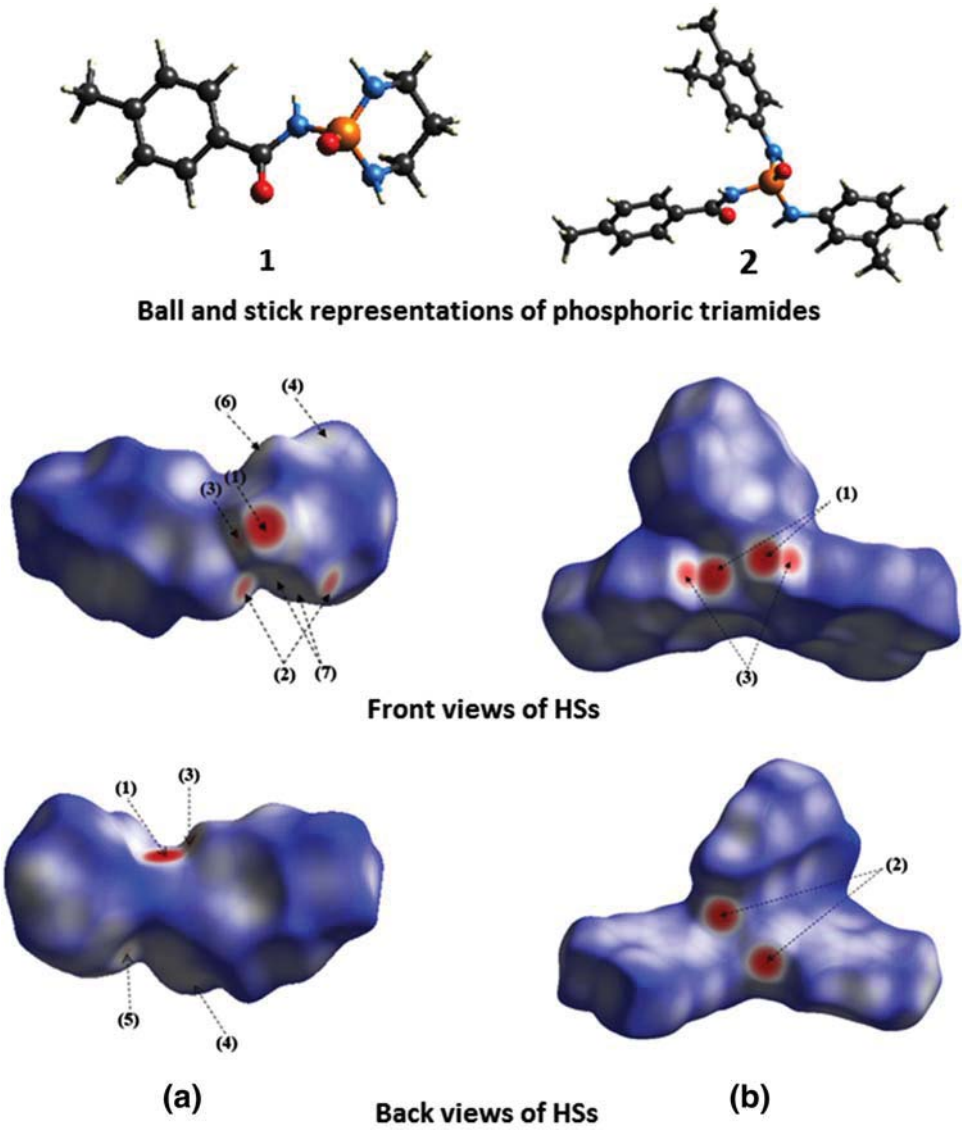

Fig. 10 Front and back views of the Hirshfeld surfaces for molecules **1** and **2** are shown in **a** and **b**, respectively. Labels on HSs are explained in Table 5

Table 5 Classical hydrogen bonds (as bold text) and other intermolecular interactions with distances shorter than the sum of van der Waals radii for **1** and **2**

Structure	D–H···A	Label	Figures
1	**N3–H3*C*···O1=P1**	**1**	10a (large red spot)
	N2–H2*C*···O2=C4	**2**	10a (large red spot)
	C6–H6···O1=P1	3	10a
	C3–H3*A*···O2=C4	4	10a
	N1–H1*C*···N2	**5**	10a
	N1–H1*C*···O2=C4	6	10a
	N2–H2*C*···N2	7	10a
2	**N1–H1···O2=P1**	**1**	10b (large red spot)
	N3–H3*B*···O1=C1	**2**	10b (large red spot)
	C3–H3*A*···O2=P1	3	10b

interaction, with the C–H from the CH_2 part. The three electron-rich π systems are present in the structure **2** and two different C–H···π interactions (as red π-holes) marked (A) and (B) are found in the crystal, as shown in Fig. 11b. In (A), one of the 3,4-$(CH_3)_2$-C_6H_3 aromatic rings acts as a source of π-electrons and in (B), 4-CH_3-C_6H_4 ring provides such electrons for aforementioned interactions. For the interactions (A) and (B), the C–H units of methyl groups in 4-CH_3-C_6H_4 and 3,4-$(CH_3)_2$-C_6H_3 groups behave as a donor, respectively.

The full fingerprint plots (FPs) of compounds **1** and **2** are illustrated in Figs. 12a and 13a, respectively. These plots represent the total interactions which can be divided into the different interactions to show contribution portions of each contact in the total Hirshfeld surfaces. For two

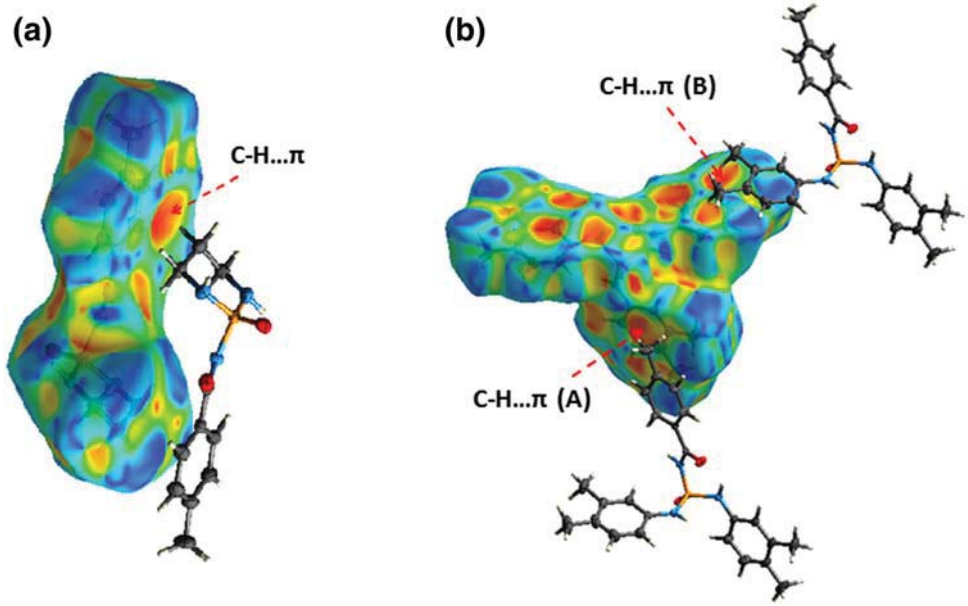

Fig. 11 Hirshfeld surfaces mapped with shape index function: **a** for **1** and **b** for **2**

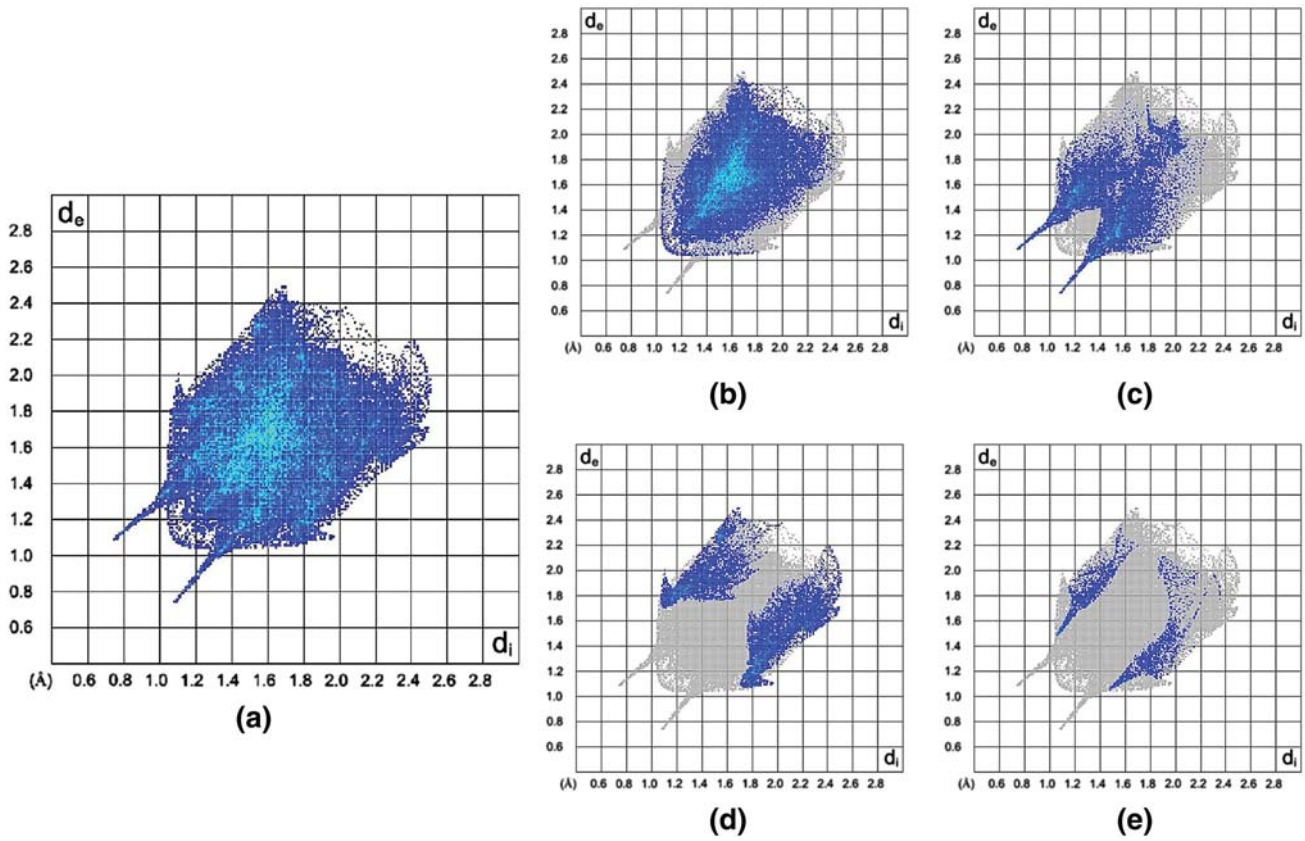

Fig. 12 Fingerprint plots for **1**. Close contacts are as follows: **a** all, **b** H···H, **c** O···H/H···O, **d** C···H/H···C and **e** N···H/H···N

structures, the H···H interactions (manifested in the middle area of the scattered points in the 2D fingerprint plots) make up the majority of the Hirshfeld surfaces (54.3 and 59.9%, Figs. 12b, 13b) relative to other contacts, as a consequence of the higher number of hydrogen atoms in these structures.

Fingerprint plots of Figs. 12c and 13c show the O···H interactions in structures **1** and **2**, with two sharp H-bond spikes in the regions of bottom right ($d_e < d_i$, O···H) and

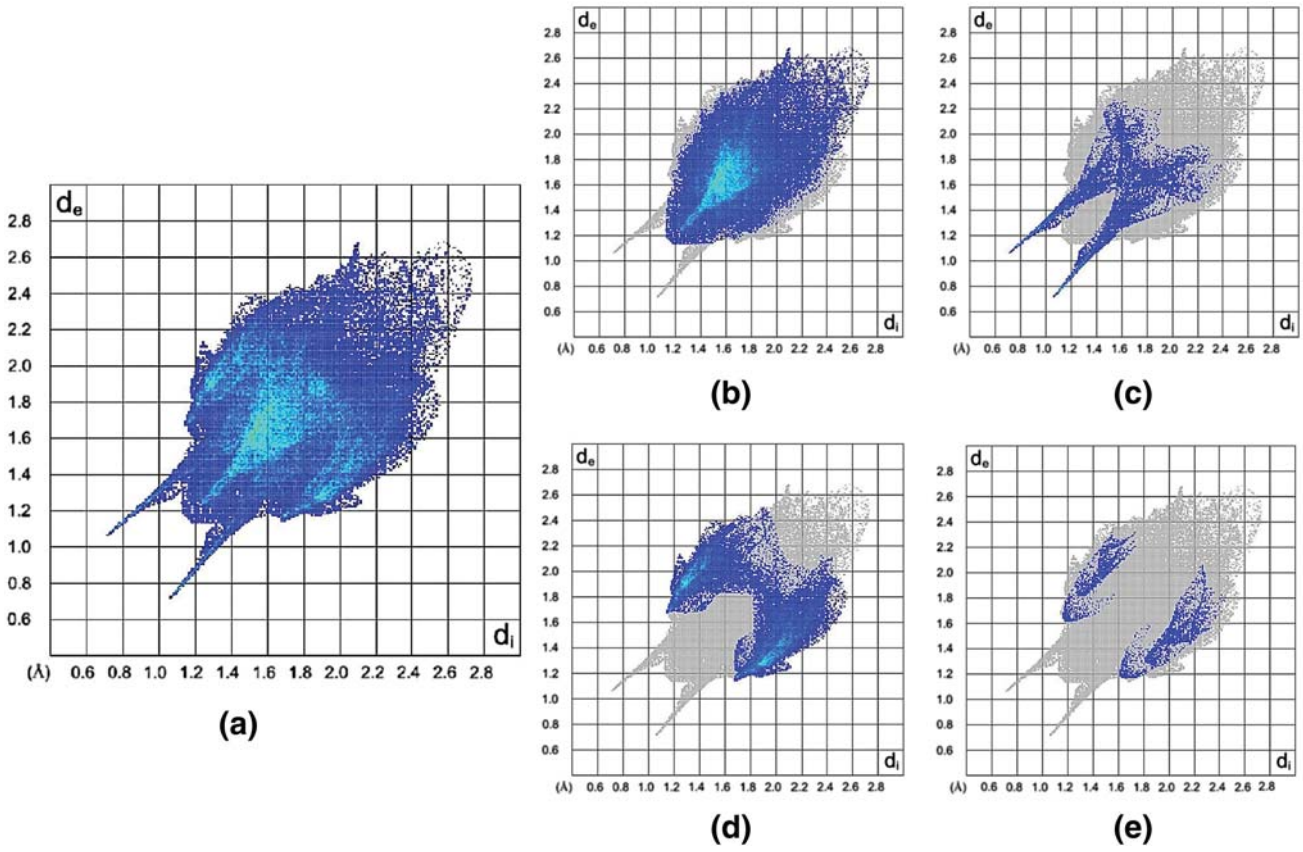

Fig. 13 Fingerprint plots for **2**. Close contacts are as follows: **a** all, **b** H···H, **c** O···H/H···O, **d** C···H/H···C and **e** N···H/H···N

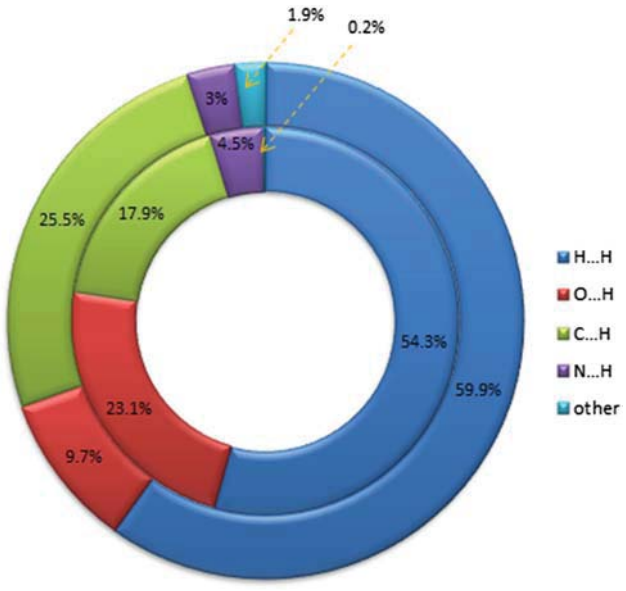

Fig. 14 Relative contributions of various intermolecular contacts for structures **1** (*inside circle*) and **2** (*outside circle*)

top left ($d_e > d_i$, H···O) of the related plots, providing the closest contacts with minimum $d_i + d_e$ values of ≈1.8 Å for both structures. The O···H interactions (23.1% for **1** and 9.7% for **2**) include both N–H···O and C–H···O contacts. As would be expected greater of O···H/H···O interactions are observed for **1**, with all of N–H units involved in the superstructure. The fewer number of unsaturated carbon atoms in **1** is also reflected in smaller C···H/H···C contacts in **1** (17.9%), as compared to **2** (25.5%), Figs. 12d and 13d.

The N···H contacts, showed in Figs. 12e and 13e, only make up 4.5% for **1** and 3% for **2**, but are significant because the nitrogen atom bonded to phosphorus has a low Lewis base characteristic and the existence of N···H interactions is a highlight of these structures, with significantly more value for the structure **1** which includes two N atoms with remarkable deviance from planarity. A comparison of Figs. 12e and 13e (for N···H contacts) indicates that the shortest $d_e + d_i$ (shown as blue points on related FPs) for **1** is near 2.6 Å and for **2** is near 2.8 Å, in which the shortest N···H contact in **1** is related to the weak intermolecular N_P–H···N_P^i interaction (N1–H1*C*···N2^i, Tables 4, 5).

In addition to the interactions discussed above, there are additional short contacts such as C···C and O···C that comprise only a small fraction of the Hirshfeld surfaces (Fig. 14) and are not shown in related fingerprint plots.

Finally, a visual inspection of FPs in Figs. 12 and 13 shows that the upper d_e and d_i values on the full FP of **1** are

more compact than those in the full FP of **2** ($d_e < 2.5$ Å and $d_i < 2.5$ Å in **1**, $d_e < 2.7$ Å and $d_i < 2.7$ Å in **2**), which indicates more efficient packing in **1**.

Conclusions

Different molecular assemblies were compared in two new structures belonging to the families of "cyclic phosphoric triamide" (**1**) and "phosphoric triamide" (**2**). Both structures include similar $C(O)NHP(O)(NH)_2$ skeleton and the differences observed in the hydrogen bond maps are driven by the following factors: (1) differences in the geometries of the nitrogen atoms bonded to the P=O group, where the N atoms with the non-planar environment in cyclic phosphoric triamide cooperate as an H-bond acceptor, but none of the N atoms in the acyclic phosphoric triamide do not take part as an acceptor; (2) different orientations of P=O versus C=O; and (3) different orientations of N–H units bond vectors. So, structures **1** and **2** are considered as models of "four-acceptor– three-donor" and "two-acceptor– three-donor". The more complicated hydrogen bond pattern of **1** and the simple hydrogen bond pattern of **2** were discussed. The details of intermolecular interactions of **1** and **2** were studied by the Hirshfeld surface analysis. The main discrepancies monitored by such analysis are related to the contribution portions of O···H/H···O contacts, in which the compound **1** not only involves the greater existence of classical hydrogen bonds but also contains the further C–H···O weak interactions. In the structure of **2**, the shortage of O···H/H···O contacts has been partially compensated by the C···H/H···C interactions, due to the greater presence of unsaturated carbon acceptors. In summary, the N atoms of diazaphosphorinane with non-planar environment lead to the engaging of more acceptors in the hydrogen bonding pattern, which results in the created diverse hydrogen-bonded motifs as well as more compacted and higher density of **1** with respect to **2** that these observations were evidenced by fingerprint plot analysis.

Acknowledgements AS and MP would like to thank the Ferdowsi University of Mashhad for financial supporting this study (Grant No. 28386/3-2013/10/02). Crystallography experiments have been supported by FriMat, University of Fribourg.

References

Allen FH, Bruno IJ (2010) Bond lengths in organic and metal-organic compounds revisited: X–H bond lengths from neutron diffraction data. Acta Crystallogr B 66:380–386. doi:10.1107/S0108768110012048

Altomare A, Cascarano G, Giacovazzo C, Guagliardi A, Burla MC, Polidori G, Camalli M (1994) *SIR92*—a program for automatic solution of crystal structures by direct methods. J Appl Crystallogr 27:435. doi:10.1107/S002188989400021X

Bauerschmidt S, Hanebeck W, Schulz KP, Gasteiger J (1992) Elucidation of reactions in the mass spectrometer. Anal Chim Acta 265:169–182. doi:10.1016/0003-2670(92)85023-Y

Braga D, Grepioni F (1997) From alkynols to alkynol complexes. A molecular assembly study. Organometallics 16:4910–4919. doi:10.1021/om970331t

Brandenburg K, Putz H (1999) DIAMOND. Crystal impact. GbR Bonn, Germany

Carletti E, Colletier J-P, Schopfer LM, Santoni G, Masson P, Lockridge O, Nachon F, Weik M (2013) Inhibition pathways of the potent organophosphate CBDP with cholinesterases revealed by X-ray crystallographic snapshots and mass spectrometry. Chem Res Toxicol 26:280–289. doi:10.1021/tx3004505

Cremer D, Pople JA (1975) General definition of ring puckering coordinates. J Am Chem Soc 97:1354–1358. doi:10.1021/ja00839a011

Desiraju G (2010) Crystal engineering: a brief overview. J Chem Sci 122:667–675. doi:10.1007/s12039-010-0055-2

Gholivand K, Madani Alizadehgan A, Mojahed F, Soleimani P (2008) Crystal structures and mass spectral fragmentation studies of some new carbacylamidophosphate compounds. Polyhedron 27:1639–1649. doi:10.1016/j.poly.2008.01.023

Gholivand K, Shariatinia Z, Mashhadi SM, Daeepour F, Farshidnasab N, Mahzouni HR, Taheri N, Amiri S, Ansar S (2009) Structural diversity in phosphoramidate's chemistry: syntheses, spectroscopic and X-ray crystallography studies. Polyhedron 28:307–321. doi:10.1016/j.poly.2008.10.057

Groom CR, Bruno IJ, Lightfoot MP, Ward SC (2016) The Cambridge Structural Database. Acta Crystallogr B 72:171–179. doi:10.1107/S2052520616003954

Hirshfeld FL (1977) Bonded-atom fragments for describing molecular charge densities. Theor Chim Acta 44:129–138. doi:10.1007/BF00549096

Macrae CF, Bruno IJ, Chisholm JA, Edgington PR, McCabe P, Pidcock E, Rodriguez-Monge L, Taylor R, van de Streek J, Wood PA (2008) *Mercury CSD 2.0*—new features for the visualization and investigation of crystal structures. J Appl Crystallogr 41:466–470. doi:10.1107/S0021889807067908

Martin AD, Britton J, Easun TL, Blake AJ, Lewis W, Schröder M (2015) Hirshfeld surface investigation of structure-directing interactions within dipicolinic acid derivatives. Cryst Growth Des 15:1697–1706. doi:10.1021/cg5016934

McKinnon JJ, Spackman MA, Mitchell AS (2004) Novel tools for visualizing and exploring intermolecular interactions in molecular crystals. Acta Crystallogr B 60:627–668. doi:10.1107/S0108768104020300

McKinnon JJ, Jayatilaka D, Spackman MA (2007) Towards quantitative analysis of intermolecular interactions with Hirshfeld surfaces. Chem Comm 3814–3816. doi:10.1039/B704980C

Metrangolo P, Resnati G (2008) Halogen versus hydrogen. Science 321:918–919. doi:10.1126/science.1162215

Michalik S, Małecki JG, Młynarczyk N (2014) Synthesis of $[Re_2Cl_4(O)_2(\mu\text{-}O)(3,5\text{-lut})_4]$ and investigation of its structure via X-ray and spectroscopic measurements and DFT calculations. Chem Pap 68:689–696. doi:10.2478/s11696-013-0493-7

Mizrahi V, Modro TA (1982) Phosphoric carboxylic imides. 1. Preparation and fragmentation behavior of dialkylphosphoryl (and phosphinyl) acetyl (and benzoyl) imides and related systems. J Org Chem 47:3533–3539. doi:10.1021/jo00139a030

Palatinus L, Chapuis G (2007) *SUPERFLIP*—a computer program for the solution of crystal structures by charge flipping in arbitrary dimensions. J Appl Crystallogr 40:786–790. doi:10.1107/S0021889807029238

Pourayoubi M, Sabbaghi F (2009) Synthesis, spectroscopic characterization and crystal structure of a new acetyl phosphorylamidate P(O)[NHC(O)C_6H_4(4-NO_2)][N($CH(CH_3)_2$)($CH_2C_6H_5$)]$_2$. J Chem Crystallogr 39:874–880. doi:10.1007/s10870-009-9582-4

Pourayoubi M, Izadyar M, Elahi B, Parvez M (2013) Combination of X-ray crystallography and theoretical study to evaluate the effect of N–H···O=P versus N–H···O=C hydrogen bonds on the N–H stretching frequencies. J Mol Struct 1034:354–362. doi:10.1016/j.molstruc.2012.10.055

Pourayoubi M, Toghraee M, Zhu J, Dušek M, Bereciartua PJ, Eigner V (2014) Database analysis of hydrogen bond patterns in phosphoric triamides completed with seven new compounds: a crystallographic and ^{15}N NMR study. CrystEngComm 16:10870–10887. doi:10.1039/C4CE01793E

Prins LJ, Reinhoudt DN, Timmerman P (2001) Noncovalent synthesis using hydrogen bonding. Angew Chem Int Ed 40:2382–2426. doi:10.1002/1521-3773(20010702)40:13<2382:AID-ANIE2382>3.0.CO;2-G

Resnati G, Boldyreva E, Bombicz P, Kawano M (2015) Supramolecular interactions in the solid state. IUCrJ 2:675–690. doi:10.1107/S2052252515014608

Sheldrick GM (2008) A short history of *SHELX*. Acta Crystallogr A 64:112–122. doi:10.1107/S0108767307043930

Sheldrick GM (2015) Crystal structure refinement with *SHELXL*. Acta Crystallogr C 71:3–8. doi:10.1107/S2053229614024218

Spackman MA, Byrom PG (1997) A novel definition of a molecule in a crystal. Chem Phys Lett 267:215–220. doi:10.1016/S0009-2614(97)00100-0

Spackman MA, Jayatilaka D (2009) Hirshfeld surface analysis. CrystEngComm 11:19–32. doi:10.1039/b818330a

Spackman MA, McKinnon JJ (2002) Fingerprinting intermolecular interactions in molecular crystals. CrystEngComm 4:378–392. doi:10.1039/b203191b

Steiner T (2002) The hydrogen bond in the solid state. Angew Chem Int Ed 41:48–76. doi:10.1002/1521-3773(20020104)41:1<48:AID-ANIE48>3.0.CO;2-U

Tarahhomi A, Pourayoubi M, Rheingold AL, Golen JA (2011) Different orientations of C=O versus P=O in P(O)NHC(O) skeleton: the first study on an aliphatic diazaphosphorinane with a *gauche* orientation. Struct Chem 22:201–210. doi:10.1007/s11224-010-9682-y

Toghraee M, Pourayoubi M, Divjakovic V (2011) Study on H-bond patterns in phosphoric triamides having a P(O)NHC(O) skeleton, a *gauche* orientation of P(O) vs C(O) in new compounds. Polyhedron 30:1680–1690. doi:10.1016/j.poly.2011.03.045

Upadhyay LSB (2012) Urease inhibitors: a review. IJBT 11:381–388

Wolff SK, Grimwood DJ, McKinnon JJ, Turner MJ, Jayatilaka D, Spackman MA (2012) *CrystalExplorer* (Version 3.1), University of Western Australia

Wu X, Hu L (2016) Design and synthesis of peptide conjugates of phosphoramide mustard as prodrugs activated by prostate-specific antigen. Bioorg Med Chem 24:2697–2706. doi:10.1016/j.bmc.2016.04.035

Yang L, Powell DR, Houser RP (2007) Structural variation in copper (I) complexes with pyridylmethylamide ligands: structural analysis with a new four-coordinate geometry index, τ4. Dalton Trans 955–964. doi:10.1039/B617136B

Yizhak RV, Znovjyak KO, Ovchynnikov VA, Sliva TY, Konovalova IS, Medviediev VV, Shishkin OV, Amirkhanov VM (2013) Synthesis and crystal structures of new dioxouranium(VI) complexes based on carbacylamidophosphates (CAPh). Investigation of extraction properties of some CAPh ligands in respect of dioxouranium(VI) nitrate. Polyhedron 62:293–299. doi:10.1016/j.poly.2013.06.043